

Preliminary assessment of a new algorithm for the MHD equations at all Mach number regimes

Carlos M. Xisto^{1a}, José C. Páscoa^{1a} e Paulo J. Oliveira^{1b}

¹Universidade da Beira Interior, Departamento de Engenharia Electromecânica, Rua Mqs D'Ávila e Bolama, 6201-001 Covilhã, Portugal. Research units: a - CAST; b - CEFT
email: xisto@ubi.pt <http://clusterdem.ubi.pt>

Abstract

In this paper we present a method for solving the compressible MHD equations at arbitrary Mach number flows. Our method is based on the well-known PISO algorithm, which is a pressure based solver. In order to handle all the possible discontinuities that can be generated by the hyperbolic system of MHD equations the AUSMPW-MHD technique is applied for the flux calculation. It allows us to obtain conservative fluxes and face values for pressure that are then inserted in the solution algorithm. Regarding validation, two sets of test cases will be addressed. The first one is the 1D Riemann problem, which is tackled using both 1D and 2D formulations for the MHD equations. The second is the 1D and 2D Alfvén waves test case, which will serve to assess the accuracy of the method in smooth flows.

Keywords: MHD; PISO; arbitrary Mach number; Riemann problem.

1 INTRODUCTION

For the numerical simulation of magnetohydrodynamic flow (MHD) two groups of algorithms have been developed. The first group was created to deal with incompressible flow [1] and the second to calculate highly compressible MHD flows [2]. However, nowadays a great number of numerical gas dynamics codes are able to solve the compressible Navier-Stokes equations at all Mach number regimes. Such algorithms are important since in the field of aerospace engineering there is often a need to solve complex flow problems that involve a wide range of Mach numbers. This is also true for the special case of MHD flow in realistic Magneto-Plasma Dynamics (MPD) thruster geometries. It is known that these devices can produce flows that range from the nearly incompressible to the hypersonic limit [3]. Still, there is a lack of solvers capable of solving efficiently the compressible MHD equations for the whole range of Mach number regimes. In the present paper we discuss an arbitrary Mach number MHD solver that is based on the PISO method. This new solver is an extension of a previous method, developed for the Euler equations [4], to the compressible MHD equations.

In the next section the numerical method is presented and the algorithm that couples all the variables is described. A special technique developed to remove the numerical errors arising from lack of satisfaction of Gauss law for the magnetic field is also briefly described. For validation two different sets of test cases are considered. The first is the 1D Riemann problem, which is tackled using both the 1D and the 2D formulation of the MHD equations. This test case will allow us to validate our algorithm for high Mach number flows ($1 < Ma < 7$) possessing discontinuities in both the velocity and magnetic fields. The second test case is the 1D and 2D circularly polarized Alfvén waves. In this final case we intend to validate our method for smooth flows at low Mach number ($Ma \approx 0.2$).

2 NUMERICAL METHOD

In this section we present the differential equations governing compressible MHD flow and describe the method used to solve that system. The algorithm developed to couple all the variables is based on the well-known PISO method [5], and is an extension of a recent method proposed by the authors for the Euler equations at arbitrary Mach number flows [4]. In the next section we present the governing equations and then the multidimensional MHD algorithm is explained in detail.

2.1 The MHD equations

Magnetohydrodynamics is related to the interaction of a conducting moving fluid with one or more magnetic fields. This interaction can be described by the MHD equations, which couple the magnetic field, given by

Maxwell equations, with the flow of a conducting fluid, ruled by the Euler equations. The ideal MHD equations are given by:

$$\frac{\partial \rho}{\partial t} + \nabla \cdot (\rho \mathbf{U}) = 0, \quad (1)$$

$$\frac{\partial \rho \mathbf{U}}{\partial t} + \nabla \cdot (\rho \mathbf{U} \mathbf{U}) + \nabla p_G - \nabla \cdot (\mathbf{B} \mathbf{B}) = 0, \quad (2)$$

$$\frac{\partial \rho e}{\partial t} + \nabla \cdot (\rho \mathbf{U} e + p_G \mathbf{U} - \mathbf{B} \mathbf{B} \cdot \mathbf{U}) = 0, \quad (3)$$

$$\frac{\partial \mathbf{B}}{\partial t} + \nabla \cdot (\mathbf{U} \mathbf{B} - \mathbf{B} \mathbf{U}) = 0. \quad (4)$$

With the magnetic field subjected to Gauss law:

$$\nabla \cdot \mathbf{B} = 0. \quad (6)$$

This system expresses the conservation of mass, momentum, total energy and magnetic field. Here we have chosen units such the vacuum magnetic permeability is equal to unity. The global pressure is given by the sum of the thermodynamic and magnetic pressure:

$$p_G = p + \frac{B^2}{2}. \quad (7)$$

The standard pressure, p , is calculated indirectly with an equation assembled using both the continuity (Eq.1) and the momentum (Eq.2) equations. Temperature is a derived quantity and is obtained through an equation of state:

$$T = \left(e - \frac{U^2}{2} - \frac{B^2}{2} \right) \frac{1}{C_v}. \quad (8)$$

2.2 Multidimensional MHD code

In this section we present the multidimensional MHD solution method. Firstly we show how the conservative fluxes are assembled by the AUSMPW-MHD technique. Then, the PISO algorithm employed in the coupling of the equations is described in some detail.

2.2.1 Conservative fluxes

The AUSMPW-MHD [6] formulation serves to calculate the set of conservative fluxes which are then assembled as the MHD system of discretized equations. For two dimensional flow exhibiting variations along the x - and y -directions, the system of equations can be written in the following conservative form:

$$\frac{\partial U}{\partial t} = \frac{\partial \mathcal{F}_x}{\partial x} + \frac{\partial \mathcal{F}_y}{\partial y}, \quad (9)$$

where U is the state vector for the conservative variables and $\mathcal{F}(U)$ is the flux function:

$$U = \begin{pmatrix} \rho \\ \rho U_x \\ \rho U_y \\ \rho U_z \\ \rho e \\ B_y \\ B_z \end{pmatrix}, \quad \mathcal{F}_x = \begin{pmatrix} \rho U_x \\ \rho U_x^2 + p_G - B_x^2 \\ \rho U_x U_y - B_x B_y \\ \rho U_x U_z - B_x B_z \\ (\rho e + p_G) U_x - B_x (B_x U_x + B_y U_y + B_z U_z) \\ B_y U_x - B_x U_y \\ B_z U_x - B_x U_z \end{pmatrix}. \quad (10)$$

With \mathcal{F}_y obtained by properly permuting indices. The global pressure and total energy are given by:

$$p_G = p + \frac{1}{2}(B_x^2 + B_y^2 + B_z^2), \quad (11)$$

$$e = \frac{1}{2}(U_x^2 + U_y^2 + U_z^2) + C_v T + \frac{1}{2\rho}(B_x^2 + B_y^2 + B_z^2). \quad (12)$$

Using the AUSM⁺ method for gas dynamics we can calculate the flux function at the cell face (index f) as follows:

$$\mathcal{F}_f = a_f(\mathcal{M}_4^+ \phi_L + \mathcal{M}_4^- \phi_R) + (\mathcal{P}_5^+ P_L + \mathcal{P}_5^- P_R), \quad (13)$$

where a_f is the common speed of sound, $\phi = (\rho, \rho U, \rho e)^T$ and $P = (0, p, 0)^T$. The subscripts L and R are the right and left side face contributions, \mathcal{M}_4^\pm and \mathcal{P}_5^\pm are Mach number interpolation functions.

In a previous paper [4] we have implemented such functions for the cell face values of velocity and pressure in a PISO method, having solved the Euler equations for an arbitrary Mach number. The purpose here is to devise a similar method of assembling the fluxes for the MHD system of equations.

The AUSM method was developed for gas dynamics using the proper characteristic speeds and, because of that, it is not readily applicable to calculate MHD flow. The main issue is that the ideal MHD equations have seven different characteristic speeds, instead of three as in the case of the Euler equations.

So, in order to properly scale the Mach number interpolation functions, we should use the weighting functions developed by [6] to account for the magnetic field. The scaled \mathcal{M}_4^\pm are then given by:

$$M_f = \mathcal{M}_4^+ + \mathcal{M}_4^- \geq 0:$$

$$\begin{aligned} \bar{\mathcal{M}}_4^- &= \mathcal{M}_4^- \cdot w \cdot (1 + f_R) \\ \bar{\mathcal{M}}_4^+ &= \mathcal{M}_4^+ + \mathcal{M}_4^- \cdot [(1 - w) \cdot (1 + f_R) - f_L], \end{aligned}$$

$$M_f < 0:$$

$$\begin{aligned} \bar{\mathcal{M}}_4^+ &= \mathcal{M}_4^+ \cdot w \cdot (1 + f_L) \\ \bar{\mathcal{M}}_4^- &= \mathcal{M}_4^- + \mathcal{M}_4^+ \cdot [(1 - w) \cdot (1 + f_L) - f_R], \end{aligned} \quad (14)$$

where f and w are functions based on the global pressure:

$$f_{L,R} = \begin{cases} \left(\frac{p_{G,L} + p_{G,R}}{p_{G,S}} - 1 \right), & p_s \neq 0, \\ 0, & elsewhere \end{cases}, \quad p_{G,S} = \mathcal{P}_5^+ p_{G,L} + \mathcal{P}_5^- p_{G,R}, \quad (15)$$

$$w = 1 - \min \left(\frac{p_{G,L}}{p_{G,R}}, \frac{p_{G,R}}{p_{G,L}} \right)^3, \quad (16)$$

with:

$$\begin{aligned} p_{G,L} &= p_L + \frac{1}{2}(B_x^2 + B_y^2 + B_z^2)_L, \\ p_{G,R} &= p_R + \frac{1}{2}(B_x^2 + B_y^2 + B_z^2)_R. \end{aligned} \quad (17)$$

In addition, the interface Mach number should be based on the fast magnetosonic speed, and not the standard sound speed, as in the AUSM⁺ method:

$$M_{L,R} = \frac{U_{L,R}}{c_f}, \quad (18)$$

where the common magnetosonic fast speed at the cell face is given by:

$$c_f = \min(c_{f,L}, c_{f,R}), \quad (19)$$

$$c_{f,L} = \left\{ \frac{1}{2} \left[a_L^2 + \frac{B_L^2}{\rho_L} + \sqrt{\left(a_L^2 + \frac{B_L^2}{\rho_L} \right)^2 - 4a_L^2 \frac{B_{n,L}^2}{\rho_L}} \right] \right\}^{\frac{1}{2}},$$

$$c_{f,R} = \left\{ \frac{1}{2} \left[a_R^2 + \frac{B_R^2}{\rho_R} + \sqrt{\left(a_R^2 + \frac{B_R^2}{\rho_R} \right)^2 - 4a_R^2 \frac{B_{n,R}^2}{\rho_R}} \right] \right\}^{\frac{1}{2}}, \quad (20)$$

where $a_{L,R}$ are the left- and right-states of the speed of sound at the cell interface and $B_n = \hat{\mathbf{S}}_f \cdot \mathbf{B}$ is the normal component of the magnetic field.

2.2.2 $\nabla \cdot \mathbf{B} = 0$ constraint

For multidimensional MHD flows special care needs to be taken to ensure that the $\nabla \cdot \mathbf{B} = 0$ constraint is satisfied or, at least, that its value is small. It has been demonstrated by Brackbill and Barnes [7] that even if this condition is satisfied at the initial time step, the numerical errors related with time and space discretization will result in the following evolution, for $\nabla \cdot \mathbf{B}$, with respect to time:

$$\frac{\partial(\nabla \cdot \mathbf{B})}{\partial t} = 0 + \mathcal{O}(\Delta x^m, \Delta t^n), \quad (21)$$

with $m, n \geq 1$. To handle this problem we use the hyperbolic/parabolic divergence cleaning method suggested by Dedner et al. [8]. They proposed coupling the $\nabla \cdot \mathbf{B} = 0$ equation to the evolution equation for \mathbf{B} by introducing a new scalar function Ψ , through a gradient term.

$$\frac{\partial \mathbf{B}}{\partial t} + \nabla \cdot (\mathbf{U}\mathbf{B} - \mathbf{B}\mathbf{U}) + \nabla \Psi = 0. \quad (22)$$

Hence an equation needs to be assembled and solved for the scalar Ψ ; in our case we have implemented the following hyperbolic/parabolic equation:

$$\frac{\partial \Psi}{\partial t} + c_h^2 \nabla \cdot \mathbf{B} + \frac{c_h^2}{c_d^2} \Psi = 0. \quad (23)$$

This equation implies that the errors associated to $\nabla \cdot \mathbf{B}$ are convected by the c_h speed and, at the same time, are damped by the dissipation coefficient c_d . The c_h speed is determined by:

$$c_h = \frac{CFL}{\Delta t \times \text{Max}\left(\frac{1}{d}\right)},$$

$$CFL = \text{Max}\left(\frac{[|U_f| + c_f]\Delta t}{d}\right), \quad (24)$$

where d is the cell size. With this approach c_h is the maximum speed that is compatible with the CFL number. The dissipation coefficient is given by:

$$c_d = \sqrt{-\Delta t \frac{c_h^2}{\ln(c_r)}}, \quad \text{with } 0 < c_r < 1. \quad (25)$$

In all our calculations we have used $c_r = 0.9$.

2.2.3 Numerical algorithm

The algorithm is based on the PISO method of Issa [5]. In a previous paper [4] we have shown how this algorithm should be extended to solve the Euler equations for arbitrary Mach number flows. In the present work we demonstrate that the algorithm may be further extended to solve the MHD equations. The algorithm uses a segregated approach with prediction and correction steps. The values obtained in the previous time step are denoted with n , and the consecutive predictions and corrections are denoted with $^{**},^{***}$.

Prediction Step, in this first step all nodal values are assumed to be known at the previous time step n . The interpolation Mach number functions are calculated at the beginning of each time step. These functions allow us to calculate the following sets of fluxes for the two dimensional MHD equations:

$$\Phi = \begin{bmatrix} \rho \\ \rho U_x \\ \rho U_y \\ \rho U_z \\ B_x \\ B_y \\ B_z \\ \rho e + p_G \\ 0 \end{bmatrix}, \quad \mathbf{P} = \begin{bmatrix} 0 \\ S_x p_G \\ S_y p_G \\ 0 \\ -\bar{B}_f U_x \\ -\bar{B}_f U_y \\ -\bar{B}_f U_z \\ -\bar{B}_f (\mathbf{U} \cdot \mathbf{B}) \\ 0 \end{bmatrix}, \quad \Phi_B = \begin{bmatrix} 0 \\ -B_x \bar{B}_f \\ -B_y \bar{B}_f \\ -B_z \bar{B}_f \\ S_x \Psi \\ S_y \Psi \\ 0 \\ 0 \\ c_h^2 B_f \end{bmatrix}. \quad (26)$$

Where $B_f = S_x B_x + S_y B_y$, with S_x and S_y being the cell face area components, and $\bar{B}_f = (B_{f,L} + B_{f,R})/2$; see [6] for more details. The flux function should be assembled as follows:

$$\mathcal{F}_f = c_f (\bar{\mathcal{M}}_4^+ \Phi_L^n + \bar{\mathcal{M}}_4^- \Phi_R^n) + (\mathcal{P}_5^+ \mathbf{P}_L^n + \mathcal{P}_5^- \mathbf{P}_R^n) + \frac{1}{2} (\Phi_{B,L}^n + \Phi_{B,R}^n). \quad (27)$$

Because we are using PISO as our algorithm we should remove the magnetic pressure from the global pressure. In this way we can calculate the face value of the thermodynamic pressure to be used in the pressure gradient term for the momentum equation (see [4]):

$$p_f^n = \mathcal{P}_5^+ p_L^n + \mathcal{P}_5^- p_R^n. \quad (28)$$

The first equation to be solved is an explicit version of the continuity equation, based on the mass flux that was previously assembled with the AUSM method. The solution of this equation will give us a prediction value for density,

$$m_f^* = c_f^n (\bar{\mathcal{M}}_4^+ \rho_L^n + \bar{\mathcal{M}}_4^- \rho_R^n),$$

$$\frac{\partial \rho^*}{\partial t} + \nabla \cdot (m_f^*) = 0. \quad (29)$$

After this an explicit equation for each direction of the magnetic field is solved. For 1D flows, with variations on the x -axis, in order to satisfy the $\nabla \cdot \mathbf{B} = 0$ condition we must guarantee that $B_x = \text{const.}$. To obey this condition we neglect the B_x equation and just solve for B_y and B_z . These equations will again use the fluxes that were previously calculated with the AUSMPW-MHD method and will allow us to obtain values for B_x^* , B_y^* , and B_z^* .

The predicted values at the present time step for the velocity field, \mathbf{U}^* , are obtained by solving an explicit version of the momentum equation. The pressure gradient and the magnetic field terms are treated in an explicit way using the previously obtained magnetic field values B_x^* , B_y^* , B_z^* , and the face values of pressure calculated with equation (28). The discretized momentum equation for \mathbf{U}^* is

$$a_p^U \mathbf{U}^* = H(\mathbf{U}^n) - \nabla p_f^n, \quad (30)$$

where a_p^U is the central velocity coefficient and the operator $H(\mathbf{U}^n)$ is build using the convective terms of neighbour cells to P and the magnetic explicit terms:

$$H(\mathbf{U}^n) = \frac{\mathbf{U}^n}{\Delta t} + S_B^* - \sum_f a_N^U \mathbf{U}_N^n. \quad (31)$$

We can then solve for the total energy (e^*) and, afterwards, the temperature T is updated using the equation of state:

$$T^* = \frac{1}{C_v} \left[e^* - \frac{1}{2} \left\{ (U^*)^2 - \frac{(B^*)^2}{\rho^*} \right\} \right]. \quad (36)$$

With this this new temperature, new values of the compressibility coefficient are evaluated, $\psi^* = \frac{1}{RT^*}$, and density is updated, $\rho^{**} = \psi^* p^n$.

Correction Step, using the $H(\mathbf{U}^n)$ operator we can calculate the velocity without the effects of pressure, see [4] for more details. The Mach number interpolation functions are again calculated inside the PISO, with the AUSMPW-MHD method (Eq.14). With these new functions, we calculate the sonic flux to be used in the pressure equation,

$$F_s^* = c_f^* (\bar{\mathcal{M}}_4^+ \psi_L^* + \bar{\mathcal{M}}_4^- \psi_R^*). \quad (32)$$

The pressure equation is built and solved using the previously obtained values for compressibility, ψ^* , and density, ρ^{**}

$$\frac{\partial(\psi^* p^*)}{\partial t} + \nabla \cdot (F_s^* p^*) - \nabla \cdot \left(\frac{\rho^{**}}{a_p^U} \nabla p^* \right) = 0. \quad (33)$$

This equation gives the predicted value for pressure, p^* . The velocity field is corrected in an explicit way using the new pressure gradient and the first predicted velocity. The pressure gradient is again calculated with the pressure face value calculated with the interpolated Mach number functions:

$$\mathbf{U}^{**} = \frac{H(\mathbf{U}^n) - \nabla p_f^*}{a_p^U}. \quad (35)$$

Finally, density is corrected, again using the equation of state, $\rho^{***} = \psi^* p^*$.

3 TEST CASES

In order to test the proposed pressure based method for compressible MHD equations of section 2 we present two types of tests. The first type of test case should allow us to assess the capability of the method to handle high Mach number flows, possessing discontinuities in both the velocity and the magnetic fields. We present solutions for the 1D Riemann problem obtained with a two dimensional grid having 256×256 nodes.

The second type of test is adequate for assessing the ability of the method to solve smooth flow cases at low Mach numbers. It comprises 1D and rotated 2D Alfvén waves, for which numerical solutions are presented and discussed.

3.1 Two-dimensional grid-aligned shock tube test cases

In both cases we set the adiabatic index to $\gamma = 5/3$ and we use a 1D box with $x \in [0,1]$ and a total of 256 nodes for the 1D case, and a 2D box with $x \in [0,1]$ and $y \in [0,1]$ with a total of 256×256 nodes for the 2D

case. These Riemann problems do not have analytical solution so, for comparison, we use the 1D results obtained with the 256 grid. In order to obtain the left- and right-face values the Minmod interpolation scheme is used.

The first test case, also considered by [9] and [10], is a 1.5D solution of a 1D Riemann problem. In Fig. 1 we present the results obtained for the MHD shock tube with a left state $(\rho, U_x, U_y, U_z, B_y, B_z, p)_L = [1, 10, 0, 0, 5/\sqrt{4\pi}, 0, 20]_L$ and a right state $[1, -10, 0, 0, 5/\sqrt{4\pi}, 0, 1]_R$, with $B_x = 5/\sqrt{4\pi}$ at $t = 0.08$. The plots show the solution for B_y , U_y , U_x and ρ on the 1D and the 2D grid. We can see that the solution captures all the known physics of the problem. In each plot we can observe, from left to right the presence of: fast shock; slow rarefaction; contact discontinuity; slow shock; fast shock.

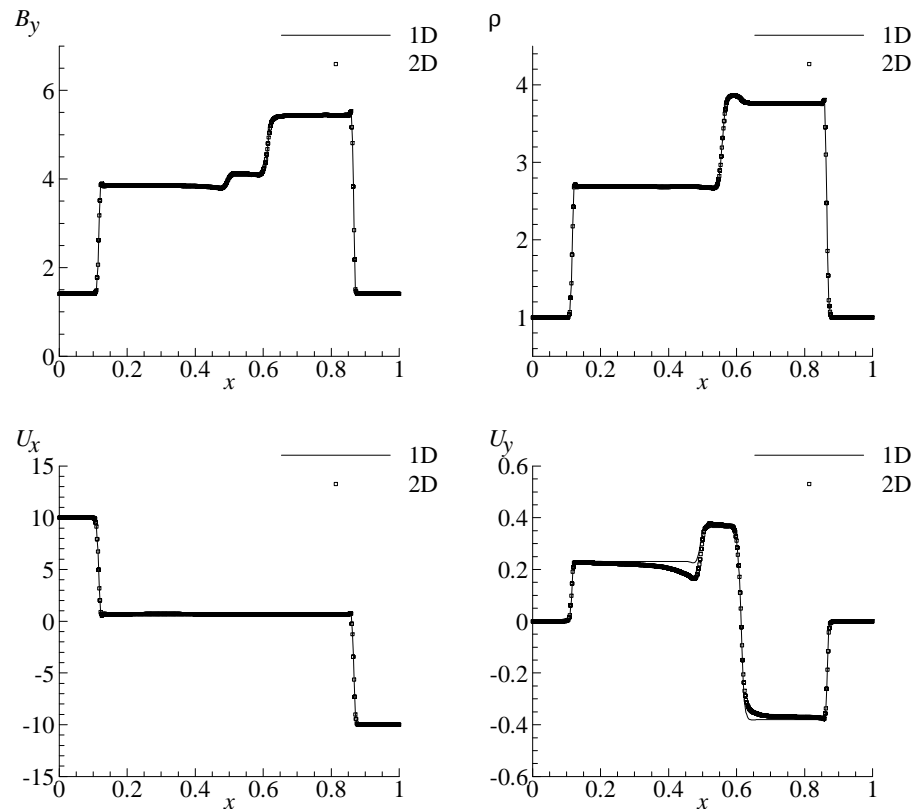


Fig.1. Solution at $t = 0.08$ of the 1.5D grid-aligned shock tube on a 256×256 grid. For comparison the 1D solution obtained in a grid with 256 cells is also plotted. The plots show, from left to right: fast shock; slow rarefaction; contact discontinuity; slow shock; fast shock.

The second test case is a 2.5D solution of the 1D Riemann problem. In Fig. 2 we present results obtained for this shock tube with left state $(\rho, U_x, U_y, U_z, B_y, B_z, p)_L = [1.08, 1.2, 0.01, 0.5, 3.6/\sqrt{4\pi}, 2/\sqrt{4\pi}, 0.95]_L$ and a right state $[1, 0, 0, 0, 4/\sqrt{4\pi}, 2/\sqrt{4\pi}, 1]_R$ with $B_x = 2/\sqrt{4\pi}$, at $t = 0.2$. The plots show results for the solution of B_y , U_y , B_z and ρ in a 1D and 2D grid. Once more our algorithm can capture all physics of the problem; from left to right: fast shock; rotational discontinuity; slow shock; contact discontinuity; slow shock; rotational discontinuity; and fast shock.

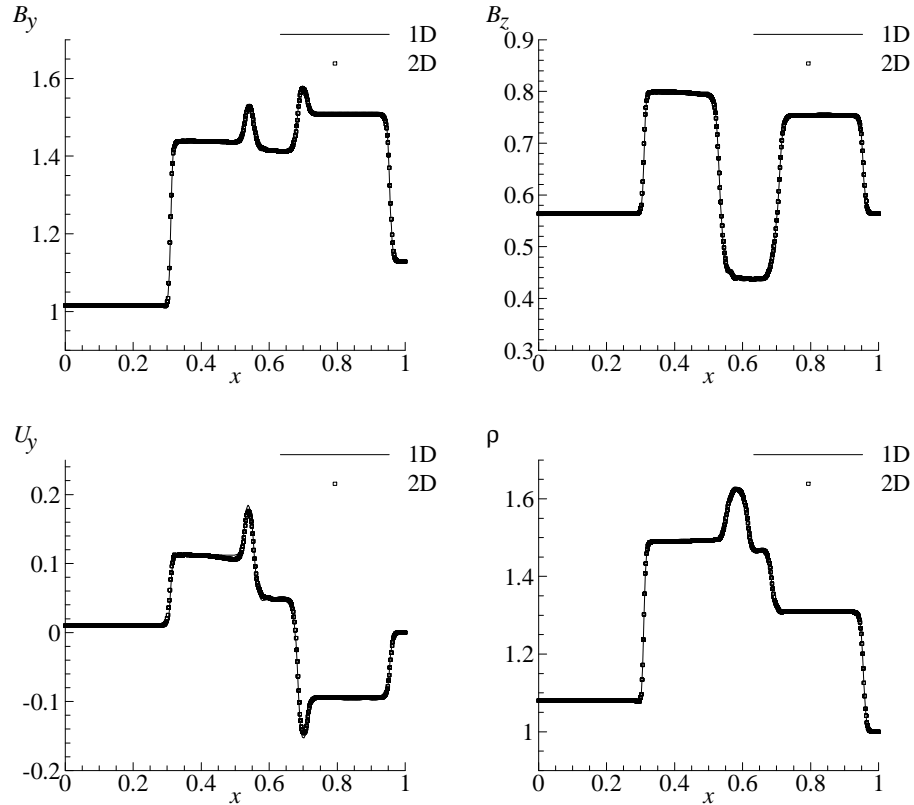


Fig.2. Solution at $t = 0.2$ of the 2.5D grid aligned shock tube on a 256×256 grid. For comparison the 1D solution obtained in a grid with 256 cells is also plotted. The plots show from left to right: fast shock; rotational discontinuity; slow shock; contact discontinuity; slow shock; rotational discontinuity; and fast shock.

3.2 Alfvén waves

The second set of test cases will allow us to validate the accuracy of our method in smooth flows. These test cases, described in [10], offer analytical solutions of the MHD equations for arbitrary amplitudes. They can be calculated using a one-dimensional formulation of the MHD equations in a 1D grid. But it is also possible to rotate the geometry at an angle α with respect to the x -axis, and in this case the problem requires a 2D solution.

The boundary conditions are periodic with $x \in [0,1]$, for the 1D case and with $x \in [0,1/\cos\alpha]$ and $y \in [0,1/\sin\alpha]$ for the 2D case. The initial conditions are: $\rho = 1$; $\gamma = 5/3$; $U_{\parallel} = 0$; $B_{\parallel} = 1$; $U_{\perp} = B_{\perp} = 0.1 \sin[2\pi(x\cos\alpha + y\sin\alpha)]$; $U_z = B_z = 0.1 \cos[2\pi(x\cos\alpha + y\sin\alpha)]$. The Alfvén speed is $|U_A| = B_{\parallel}/\sqrt{\rho} = 1$, in $t = 1$ the flow is expected to return to its initial state. The x and y components of the magnetic field are given by: $B_x = B_{\parallel}\cos\alpha - B_{\perp}\sin\alpha$; and $B_y = B_{\parallel}\sin\alpha + B_{\perp}\cos\alpha$ (similarly for velocity). As expected, for 1D flow $B_x = B_{\parallel}$ and $B_y = B_{\perp}$.

In Fig.3 we present the results predicted for the magnetic field components, for the 1D case ($\alpha = 0$) with a grid resolution of $N = 64$, which shows that after five periods, both B_y and B_z components return to their initial state. This is expected because in 1D the B_x is a constant and we do not have any errors associated to $\nabla \cdot \mathbf{B}$. At the same time it is proved that the numerical method does not introduce any errors for this kind of smooth flows.

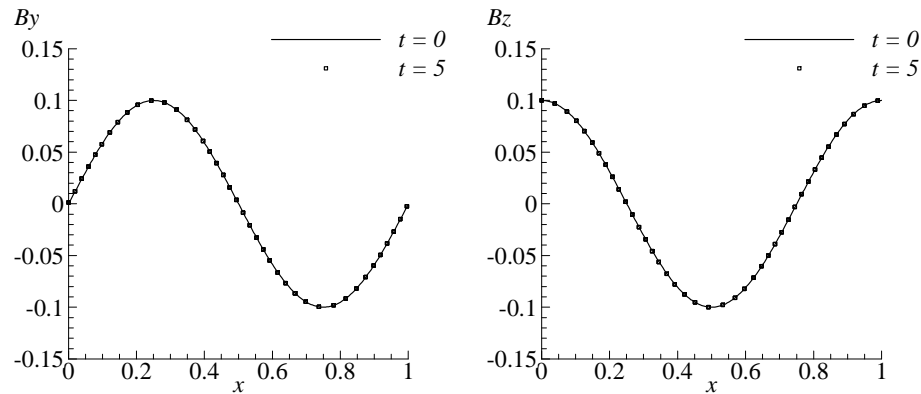


Fig.3. Results for the 1D Alfvén wave test case. The plots show the y- and z-component of the magnetic field after five periods. For comparison we also plot the initial state for both variables.

The second test is the corresponding 2D case which is solved on a $N \times N$ grid making an angle $\alpha = 30^\circ$ with the x -axis. We have performed this test with three different grid resolutions: $N = 64$; $N = 32$; $N = 16$. In Fig. 4 we present the results for the perpendicular component of the magnetic field vector projected against a vector parallel to the direction of the wave propagation $r_{\parallel} = x \cos \alpha + y \sin \alpha$. We plot the solution obtained on the three grid resolutions after five periods. For comparison we also plot the initial value on the $N = 64$ grid. As we can see, on the finest grid, for $N = 64$, the magnetic field returns to its initial state, as expected. However, if we decrease grid resolution, the errors related to $\nabla \cdot \mathbf{B} \neq 0$ propagate and sum up destroying the cyclic repeatability of the numerical solution. This was expected since we have shown that these errors are related with space discretization.

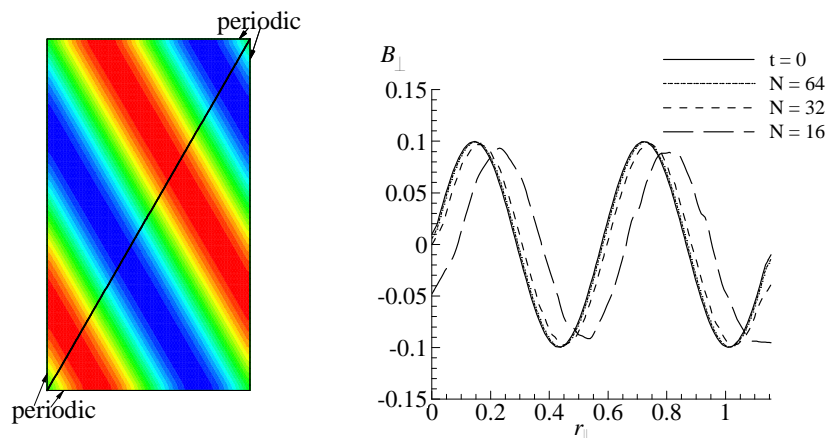


Fig.4. Results for the 2D Alfvén wave test case. *Left*: Boundary conditions and initial distribution of the perpendicular component of the magnetic field $B_{\perp} = B_y \cos \alpha - B_x \sin \alpha$. *Right*: The plot shows B_{\perp} after five periods ($t = 5$) projected against a vector parallel to the direction of the wave propagation. The full line shows the initial distribution calculated on the $N = 64$ grid.

4 CONCLUSIONS

In this work we have described a method for the simulation of compressible MHD flows. The results for the shock tube problem demonstrated that a pressure based algorithm can calculate highly compressible MHD flow, including the complex discontinuities that are associated to this hyperbolic system of equations. We have also shown that the method can solve smooth flows with accuracy. However, further tests will be needed to assess the accuracy of this method in the calculation of incompressible MHD flow.

It is also important to test this algorithm with an enlarged set of complex and realistic test cases. For the incompressible flow the Hartman test case (see [11]) can be considered and, for the compressible flow, the low- β cylinder problem [12] could be used as test case.

5 ACKNOWLEDGEMENTS

This work was supported by FCT grant SFRH/BD/60285/2009 and by FCT project PTDC/CTESPA/114163/2009 “SpaceProp - MHD Numerical Modeling in nozzles of MPD Thrusters for Space Propulsion”. Additional financial support was provided by CAST - Center for Aerospace Science and Technology at UBI.

REFERENCES

1. M. Ni, R. Munipalli, P. Huang, N. Morley, M. Abdou, A current density conservative scheme for incompressible MHD flows at a low magnetic Reynolds number. Part II: On an arbitrary collocated mesh, *Journal of Computational Physics*, 227(1), 205-228, 2007.
2. S. Li, An HLLC Riemann solver for magneto-hydrodynamics, *Journal of Computational Physics*, 203(1) 344-357, 2005.
3. H. Takeda, S. Yamamoto, Numerical Investigation of Supersonic MPD Viscous Flows with Ionization, *JSME International Journal Series B*, 45, 97-101, 2002.
4. C. M. Xisto, J. C. Páscoa, P. J. Oliveira, D. A. Nicolini, A hybrid pressure-density-based algorithm for the Euler equations at all Mach number regimes, *International Journal for Numerical Methods in Fluids*, 2011, in press, doi:10.1002/fld.2722..
5. R. I. Issa, Solution of the implicitly discretized fluid flow equations by operator-splitting, *Journal of Computational Physics*, 62, 40-65, 1986.
6. S. H. Han, J. I. Lee, K. H. Kim, Accurate and robust pressure weight advection upstream splitting method for magnetohydrodynamics equations, *AIAA Journal*, 47(4), 970-981, 2009.
7. J. U. Brackbill, D. C. Barnes, The effect of nonzero $\nabla \cdot \mathbf{B}$ on the numerical solution of the magnetohydrodynamic equations, *Journal of Computational Physics*, 35, 426-430, 1980.
8. A. Dedner, F. Kemm, D. Kröner, C.-D. Munz, T. Schnitzer, M. Wesenberg, Hyperbolic divergence cleaning for MHD equations, *Journal of Computational Physics*, 175, 645-673, 2002.
9. D. Ryu, T. W. Jones, A. Frank, Numerical magnetohydrodynamics in astrophysics: algorithm and tests for multidimensional flow, *The Astrophysical Journal*, 452, 785-796, 1995.
10. G. Tóth, The $\nabla \cdot \mathbf{B} = 0$ constraint in shock-capturing magnetohydrodynamics codes, *Journal of Computational Physics*, 212(2), 617-636, 2000.
11. J. Páscoa, F. Brójo, J. Monteiro, Numerical simulation of magneto-plasma thrusters for aerospace propulsion using MHD formulation, *Proc. 14th International Conference on Emerging Nuclear Energy Systems*, Lisbon, paper O-7.2, 6 pgs, 2009.
12. H. D. Sterk, B. C. Low, Complex magnetohydrodynamic bow shock topology in field-aligned low- β flow around a perfectly conducting cylinder, *Physics of Plasma*, 5(11), 4015-4027, 1998.